Dry air cyclic oxidation of mixed Y/Yb disilicate environmental barrier coatings and bare silica formers

P. Stack[†], M. Sweet[‡], C. Parker[§], M. Lance[§], M. Ridley[§] B. Pint[§], K. Kane[§]

[†]College of Engineering, University of Akron, Akron, OH

[§] Materials Science and Technology Division, Oak Ridge National Laboratory, Oak Ridge, TN

[‡]Praxair Surface Technologies, Indianapolis, IN

Abstract

Mixed Y and Yb disilicate coatings (Y/Yb)DS have been proposed as dual function thermal and environmental barrier coatings (EBCs) for protecting SiC-based ceramic matrix composites in gas-turbine environments. As an initial step, the 1350°C dry air cyclic oxidation of atmospheric plasma sprayed ($Y_{1.2}$/$Yb_{0.8}$)DS and ytterbium disilicate/ytterbium monosilicate (YbDS/YbMS) EBCs deposited onto Si bond coatings was compared. As a baseline for evaluating EBC oxidant permeability, the dry air cyclic oxidation scale growth rates for bare silica formers (SiC, Si) were also measured and were consistently higher than rates previously measured after isothermal oxidation. Regarding Si bond coat oxidation rates underlying (Y/Yb)DS and YbDS/YbMS EBCs, the thinner silica scale formed under the thinner and denser (Y/Yb)DS coatings suggested a lower oxidant permeability than YbDS/YbMS. After 500 1-h cycles, the (Y/Yb)DS coating was comprised of only the β-polymorph disilicate and minor amounts of the X-2 phase monosilicate phase. Negligible differences in oxidation kinetics for (Y/Yb)DS coatings over the 90 – 240 µm thickness range were observed.

Introduction

SiC-based ceramic matrix composites (CMCs) are an attractive class of high temperature structural materials due to low rates of oxidation[1] and excellent high temperature strength [2, 3]. However, in high pressure and high velocity environments containing water vapor like gas-turbines, SiC oxidizes in a paralinear manner[4] owing to the competing processes of water vapor enhanced silica formation[5, 6] and silica volatilization[7, 8]. To prevent component recession, SiC-based CMCs are coated with environmental barrier coatings (EBCs)[9–19] which mitigate scale volatilization while simultaneously inhibiting water vapor enhanced rates of oxidation[20, 21]. Although having already achieved commercial success in the aerospace sector[22], there are still large gaps in the literature regarding performance and failure mechanisms of EBCs[23].

The current generation of EBCs are typically comprised of a ytterbium disilicate (YbDS) top coating deposited onto a Si bond coating[23–28], where both coatings are applied via atmospheric plasma spraying (APS)[29, 30]. YbDS is selected as a top coating due to its low coefficient of thermal expansion mismatch with SiC[24, 30], excellent chemical compatibility, seemingly low rate of oxidant permeability [24], and lower rates of silica activity compared to SiO_2 scales [i.e. volatilization] [31]. However, YbDS still experiences minor volatilization rates at lower gas velocities [24] and detrimental volatilization rates at higher velocities [32]. Thus, alternative top coating materials are being evaluated.

From a thermomechanical perspective, most single component rare-earth disilicates (REDS) other than YbDS are viewed as unsuitable due to high coefficient of thermal expansion (CTE) mismatch with SiC-based materials [11, 33] and/or exhibiting phase transformations at gas-turbine relevant temperatures[34, 35]. However, studies have shown that judicious fabrication of multicomponent rare-earth disilicates (REDS)[35–40] may offer coatings exhibiting a primarily single-solution ß-phase composition and tailorable properties like CTE and thermal conductivity. As a nearer term application, Turcer *et al.* have shown that two-component Y/Yb disilicates have lower thermal conductivities than YbDS[35, 40], which may lower the bond coating temperature and thereby extend coating lifetimes. Based off Fernandez-Carrion *et al.'s* earlier experimental work [41], a $(Y_{1.2}/Yb_{0.8})$DS composition is expected to exhibit a single ß-phase up to approximately 1650°C.

Many researchers are working to understand O diffusion across EBCs [42–48]. Zhao *et al.* combined atomistic modelling and O tracer diffusion studies to suggest that shortened bond lengths in ß-REDS crystal structures may lead to lower rates of O lattice diffusion [47]. Additionally, modeling work by Sullivan indicated that EBC thickness may have a pronounced role on the underlying silica formation kinetics[48]. Thus, during air oxidation, mixed (Y/Yb)DS EBCs could have a lower overall O permeability than solely YbDS EBCs, and varying EBC thickness may impact oxidation kinetics.

In the current study, the 1350°C dry air cyclic oxidation of a mixed APS $(Y_{1.2}/Yb_{0.8})$DS coating was compared to a APS YbDS/YbMS[20, 25] coating. To evaluate both coating's impact on underlying rates of Si bond coating oxidation, the silica scale growth rates during cyclic oxidation of bare silica formers (SiC, Si) also were measured for comparison. (Y/Yb)DS coatings were also deposited at varying thicknesses to study the effect of coating thickness on scale growth rate. X-ray diffraction was used to investigate the stability of the mixed silicate coating during thermal cycling at 1350°C.

Experimental details

Mixed $(Y_{1.2}/Yb_{0.8})$DS coatings were deposited at Praxair Surface Technologies (Indianapolis, IN) with APS. Chemically vapor deposited (CVD) SiC (Dow Chemical, 99.99% purity) coupons (10x20x2mm) with a ~2mm through hole for sample suspension and chamfered edges were grit-blasted with SiC and subsequently coated on one face with a Si bond coating (nominally ~70 µm). (Y/Yb)DS top coatings were deposited at three different thicknesses: 90, 160, and 240 µm. No annealing step was performed after deposition. The YbDS/YbMS coatings (formerly referred to as YbDS[20, 25, 49] were deposited by APS at the Center for Thermal Spray Research, (Stony Brook, NY). Coatings were deposited on similar CVD SiC coupons, also grit-blasted with SiC and subsequently coated on one face with a ~60 µm thick Si bond coat, and then deposited with a ~180 µm YbDS/YbMS coating and annealed for 4 h at 1300°C in air to increase coating crystallinity[25, 50]. No annealing step was necessary for the (Y/Yb)DS coatings. The microstructures of the two EBCs will be discussed below.

The coated coupons, bare Si (Dow Chemical, 99.99% purity, 17 mm OD x 2 mm thickness) and CVD SiC coupons were subjected to 1-h furnace cycle testing (FCT) at 1350°C in dry air. A cycle consisted of 1 h at temperature followed by 10 min cooling with flowing dry air (~130 mL/min) in the reaction tube. The cyclic rig utilizes an alumina reaction tube, with over ~15 kh of exposure time at temperatures >1300°C. After FCT, coupons were cross sectioned, embedded in resin, and metallographically prepared with a final colloidal silica polish. Cross-sectional back-scatter electron microscopy was performed with a Tescan Mira3 operating at 10kV. Raman Spectroscopy was performed with an inVia Raman Microscope (Renishaw) using a 532 nm laser. XRD was collected with a Panalytical X'pert diffractometer utilizing MoKα radiation. Scale thickness was determined with a semi-automated Python-based image analysis method developed at ORNL[20, 51, 52], called Size of Oxidation Feature Image Analysis (SOFIA), which enables thousands of reaction layer thickness measurements to be made from a single micrograph.

Results and Discussion

Dry air isothermal and cyclic oxidation rates of silica formers

The cyclic and isothermal rates of dry air oxidation of SiC (red) and Si (green) are compared in Figure 1. Rate constants, k_p ($\mu m^2/h$), were calculated assuming parabolic kinetics[20, 53, 54] with

$$X^2 = k_p t,$$

where x is scale thickness in μm and t is exposure time in hours. The rate constants in Figure 1 were calculated from scale thicknesses measured at single times (fit to the origin; will include transient oxidation) as opposed to steady-state rates that are calculated from thicknesses measured at several times[6, 20, 49, 54] (not fit to the origin; will not include transient oxidation). Cross sections were not taken at multiple times, so the single exposure times used in Eq. (1) are included as data labels in Figure 1.

The isothermal oxidation rates of SiC and Si were previously found[20] to be in excellent agreement with rates determined by Ogbuji and Opila[54] and the projected rates of Deal and Grove[53], respectively. At 1250°C, the isothermal rates of SiC and Si are almost two orders of magnitude lower than the rates of alumina formation on Pt-NiAl coatings determined by Smialek [55]. The cyclic rates of SiC and Si oxidation (filled symbols) were marginally higher than the isothermal rates (the activation energy of the Si isothermal rates over 1250°-1350°C was used to project the FCT Si oxidation rate down to 1250°C). Raman spectroscopy identified cristobalite as the sole crystalline reaction product, indicating that alumina reaction tube impurity driven tridymite formation[56] was not responsible for the accelerated rates. The higher cyclic rates conflicts with the earlier findings of Opila *et al.*[57], who reported that dry air cyclic and isothermal rates of SiC and Si_3N_4 were nearly identical at 1300° and 1500°C. However, Opila *et al.* utilized specimen mass change to calculate rate constants and only compared 5-h cyclic and isothermal exposures up to 50 h, while the current study calculated rates from scale thickness and performed 1-h cycling up to 500 h. A possible explanation for the increased rates with cyclic oxidation is scale cracking due to the cristobalite phase transformation and associated stresses (estimated as 10^1-10^2 GPa[58]) and/or thermal transient scale stresses. Vertical "channel-cracks" [24] could provide short-circuit diffusion pathways that accelerate growth. During thermal cycling in steam of α-SiC, Kowalski and Harder observed slightly increased oxidation rates with increased rates of cycling[59] and attributed it to earlier cracking leading to thicker scales. Utilization of the dry air oxidation rates of Si (a framework developed by Harder[21] and recently repeated[20]) creates a baseline to assess the impact of an EBC on reducing dry air cyclic oxidation. Different conclusions are reached based on what base line (isothermal or cyclic) is used.

Crystallographic microstructure of the (Y/Yb)DS coating

XRD patterns of the (Y/Yb)DS coating in the as-sprayed condition and after 500 1-h cycles in dry air at 1350°C are reported in Figure 2(a) and Figure 2(b), respectively. After deposition, the high background suggests the coating was comprised of amorphous and a solid-solution lattice expanded β-YbDS phase, the latter being strongly evidenced by the shifted lattice reflections from 2θ = 32.5-34.0. No prominent monosilicate peaks were detected. After dry air FCT, the coating became highly crystalline, being primarily composed of the solid-solution β-phase and a small amount of yttrium monosilicate, suggesting the β-phase is stable during thermal cycling at 1350°C in air. Regarding the monosilciate phase, a solid solution (Y/Yb)MS cannot be ruled out presently. Due to poor x-ray penetration depth, quantification of the disilicate:monosilicate ratio was determined via image analysis, and will be discussed below.

Comparison of (Y/Yb)DS and YbDS/YbMDS microstructure after FCT

Cross sectional BSE micrographs of the (Y/Yb)DS-90µm and YbDS/YbMS-180µm samples after 500 1-h cycles in dry air at 1350°C are shown in Figure 3(a) and Figure 3(b), respectively. The microstructure of the (Y/Yb)DS and YbDS/YbMS coatings were dramatically different, the former being highly dense and the latter possessing large pores and splat boundaries. The darker gray contrast regions of the coating are the disilicate phase, while the lighter contrasted regions are monosilicate[24, 25]. Image analysis of the three different (Y/Yb)DS coating thicknesses (90, 160, 240 µm) found no appreciable differences in either monosilicate content or porosity over the course of thermal cycling. For the (Y/Yb)DS coating, the DS:MS ratio was ~93:7 and porosity was 4.8±2.5 vol.%. Conversely, the DS:MS ratio for the YbDS/YbMS coating was 6:4, and porosity was 9.7±1.6 vol.%. Also, the YbDS/YbMS coating visibly contains more microcrack networks with potentially varying degrees of through-coating continuity. Higher magnification BSE micrographs of the top coating-bond coating interfaces show the formed TGOs in Figure 3(c) and Figure 3(d) of both EBC types. Even with a thicker silicate coating, the YbMS/YbDS sample formed a visibly thicker TGO than the (Y/Yb)DS sample.

(Y/Yb)DS and YbDS/YbMS kinetics

Median TGO thickness values for (Y/Yb)DS for the 90, 160, 240 µm coatings after 100, 300, and 500 1-h cycles at 1350°C in dry air are plotted against the square root of time in Figure 4(a) (assuming parabolic kinetics). The error bars for each measurement are the 25-75% inner quartile range (IQR). At each time, all measured mixed silicate TGO thicknesses were identical within the error range. The calculated steady-state parabolic rates (determined from the slopes of the dashed lines, not including transient stage up to 100 h) for the 90, 160, and 240 µm thick coatings were 1.2E-3, 1.4E-3, and 3.2E-3 $\mu m^2/h$, respectively. Although the fastest rate was determined for the 240 µm thick coating, because scale thicknesses at each time were nearly indistinguishable, the differences in calculated rate are deemed insignificant. Therefore, all three thicknesses are viewed as resulting in similar oxidation kinetics up to 500 1-h cycles in air at 1350°C. The TGO thickness of the YbDS/YbMS sample at 500 h is also shown. Although the IQR of the YbDS/YbMS scale thickness overlaps those of the (Y/YbDS), the difference in median is larger than the relative differences between the (Y/Yb)DS samples.

Rate constants can be calculated from single times (utilizing Eq. 1) but using multiple times generates a steady-state rate. This difference is shown in Figure 4(b), where rates determined from the scale thicknesses of the (Y/Yb)DS-90µm sample at 100, 300, and 500 h are plotted as hollow symbols, while the steady-state rate over 100-500 h is plotted as a filled symbol; the steady-state rate, which does not include transient oxidation, is lower than all the single-time rates, stressing the important of utilizing steady-state rates when projecting thickness evolution over time. Although steady-state rates were not determined for the YbDS/YbMS EBC, comparisons of the 500 h rates indicate that the (Y/Yb)DS EBC exhibited a lower growth rate than the YbDS/YbMS EBC.

Another identical YbDS/YbMS sample was subjected to 500 1-h cycles in dry air at 1300°C and the resultant rate was identical to the dry air isothermal rate of Si, Figure 4b. In a similar vein, the steady-state rate of dry air cyclic oxidation of a YbDS coating reported by Lee[23] is also nearly identical to the isothermal rate. If the isothermal rates of Si oxidation are utilized as the baseline (green dashed line), one could conclude that only the (Y/Yb)DS coating had a significant impact on reducing dry air cyclic oxidation rates. However, if instead, the cyclic rates of bare Si oxidation (solid green line) are utilized, then all three EBCs, the (Y/Yb)DS, YbDS/YbMS, and YbDS coatings, reduce the oxidation rate of the underlying Si bond coatings but to varying degrees. The activation energy of the isothermal rates of bare Si oxidation was utilized to extrapolate the mixed silicate (Y/Yb)DS steady-state rate down to 1316°C, resulting in an order of magnitude lower TGO growth rate than the steady-state rate of YbDS[23].

All of the (Y/Yb)DS coatings showed lower scale growth rates than the 180 µm YbDS/YbMS coating during 1-h cycling at 1350°C. This could be attributed to a change in diffusion rate or mechanism through the TGO but a number of literature results suggest differences in EBC permeability are responsible. Vassen *et al.* deposited YbDS coatings with well controlled variations in coating porosity and correlated density with reduced oxidation in air[26]. Comparatively, Richards *et al*.[24] reported relatively slow-growing steam oxidation kinetics for YbDS coatings (Figure 4(b), purple triangle), while Lee, under identical testing parameters, reported kinetics over an order of magnitude faster (red triangle)[23], and attributed the differences to coating density. The (Y/Yb)DS coating is significantly denser than the YbDS/YbMS coating. Conversely, Zhao *et al.*[47] compared lattice O diffusion of β-YbDS and β-ScDS (scandium disilicate) with tracer diffusion studies, and combined with atomistic modeling, attributed the lower rates of O lattice diffusion through ScDS to the smaller atomic bonds compared to YbDS. Presently, the mixed (Y/Yb)DS silicate structure, Figure 2, exhibits larger bond lengths than YbDS, and thus should possess higher rates of O lattice diffusion. However, Wada and Matsudaira *et al.* [42, 43] revealed that the oxygen permeation contribution from grain boundary diffusion is orders of magnitude higher than lattice diffusion, and furthermore that under oxygen pressure differentials similar to the present EBC oxidation experiments, oxygen diffusion coefficients at YbMS-YbMS grain boundaries are higher than at YbDS-YbDS grain boundaries, 1.2E-13 and 5.2E-14 m^2s^{-1}, respectively[43]. Thus, coatings with decreased concentrations of the monosilicate phase, such as the (Y/Yb)DS coatings in this study, may experience slower TGO kinetics due to the order of magnitude decrease in oxygen grain boundary diffusivity for YbDS compared to YbMS. The results of this work suggest that the starting EBC microstructure and its evolution with respect to time are more likely to reduce TGO growth rates for extended hours in service than simply increasing the EBC thickness.

Although the present air oxidation experiments appear less relevant from an application standpoint where H_2O (g) is present, the findings indicate the complexity associated with EBC performance without the further complication of H_2O (g) effects on scale growth. For example, the mechanical implications of a highly dense EBC are not understood. A porous microstructure may allow greater strain tolerance but increased permeability. Also, if EBC chemistry and phase composition strongly influence permeability and therefore TGO growth rates, there may be tradeoffs between permeation and other properties such as CTE, volatilization, thermal conductivity and resistance to CMAS. The very low rates observed may be useful for other applications such as coatings for ultra-high temperature ceramics[1]. The coupling effects of porosity, grain size, and EBC phase boundaries on TGO growth rates remain an important topic for exploration of novel EBC architectures.

Experimentation is also needed to investigate if cyclic steam oxidation rates of bare silica formers are higher than isothermal steam rates, as an earlier report relies on steam isothermal rates to evaluate EBC effectiveness[20], where effectiveness is deemed the propensity to reduce steam oxidation rates. The steady-state rate at 1350°C of a YbDS/YbMS sample in 90vol%H_2O/10vol%air[20] (filled brown triangle, Figure 4) was previously calculated to be proportional to the isothermal rate of bare Si in ~6vol%H_2O-air balance. This was done by extrapolating the steam isothermal oxidation rate of bare Si down to lower P_{H2O} environments. If the cyclic steam oxidation rates are higher than isothermal rates, then a similar extrapolation to lower P_{H2O} environments would calculate a more effective EBC than previously reported.

Conclusions

Dry air cyclic oxidation of bare silica formers and multilayer Si/RE-silicate EBCs was conducted to investigate TGO formation rates in (Y/Yb)DS and YbDS/YbMS EBCS. For bare SiC and Si, the cyclic oxidation rates were higher than previously measured rates in isothermal oxidation. After 1350°C cyclic exposures, the (Y/Yb)DS coating was highly crystalline, being comprised of a solid-solution lattice expanded YbDS phase and a small amount of YMS. Calculation of TGO thicknesses for both EBC variants found that the significantly denser (Y/Yb)DS EBC reduced dry air cyclic oxidation rates more than the 180 µm YbDS/YbMS coating. No significant difference in kinetics was observed when the (Y/Yb)DS coating thickness was 90, 160, or 240 µm.

Acknowledgements

The authors would like to thank E. Garcia and S. Sampath from the Center for Thermal Spray Research, Stony Brook University, and to V. Cox, T. Geer, C. O'Dell, B. Johnston, G. Garner, J. Wade, from ORNL. The authors would also like to thank Y. Su and D. Sulejmanovic for technical review at ORNL, and B. Harder from NASA for helpful comments on data analysis. Access to the Raman spectrometer was provided by the Nuclear Nonproliferation Division at ORNL. This work was funded by the Advanced Turbine Program (managed by R. Dennis at NETL), Office of Fossil Energy, Department of Energy.

Figures

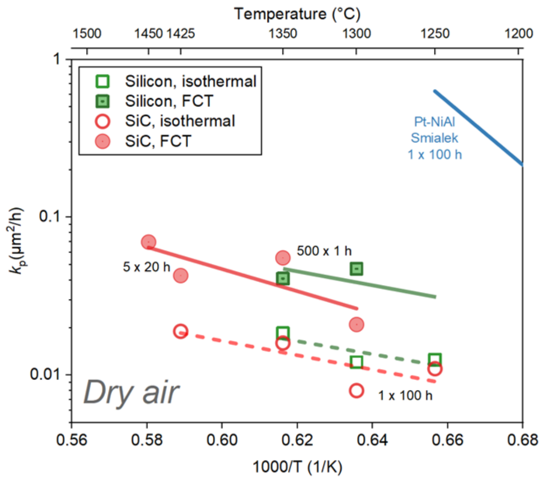

Figure 1 Arrhenius plot of rates of silica formation on bare CVD SiC (red circles) and bare silicon (green squares) after isothermal (hollow) and FCT (filled) dry air exposures. All exposure lengths are labelled. Isothermal exposures were performed in a SiC reaction tube[20, 58] and FCT exposures were performed in thoroughly aged alumina reaction tubes. Rates of isothermal alumina formation on Pt-NiAl coatings from Smialek[55] are shown in blue.

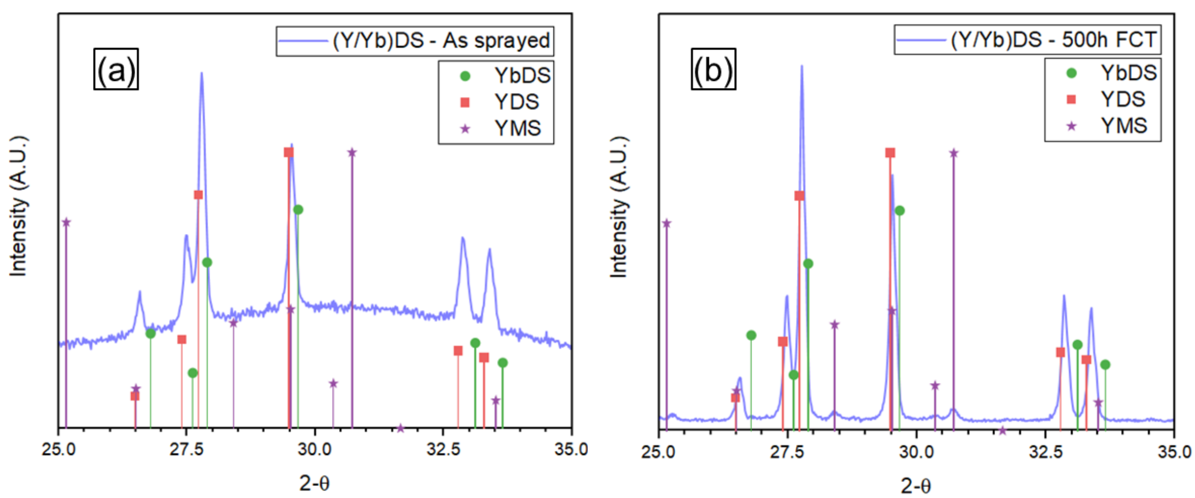

Figure 2 XRD pattern of ($Y_{1.2}$/$Yb_{0.8}$)DS coating in the (a) as-sprayed condition and (b) after 500 1-h cycles in dry air at 1350°C.

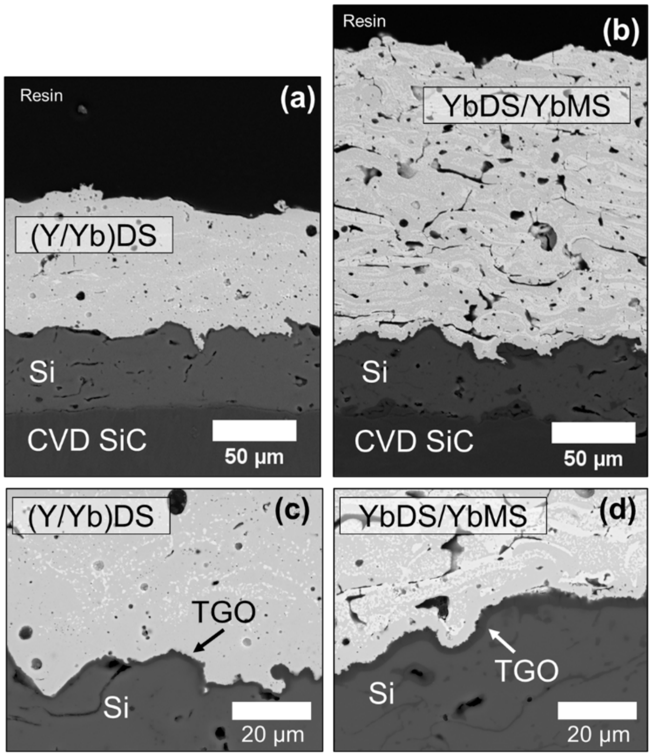

Figure 3 Cross sectional BSE micrographs of (a) (Y/Yb)DS-90µm and (b) YbDS/YbMS-180µm samples after 500 1-h cycles at 1350°C in dry air, and higher magnification BSE micrographs showing the formed silica TGO of the (c) (Y/Yb)DS and (d) YbDS/YbMS samples.

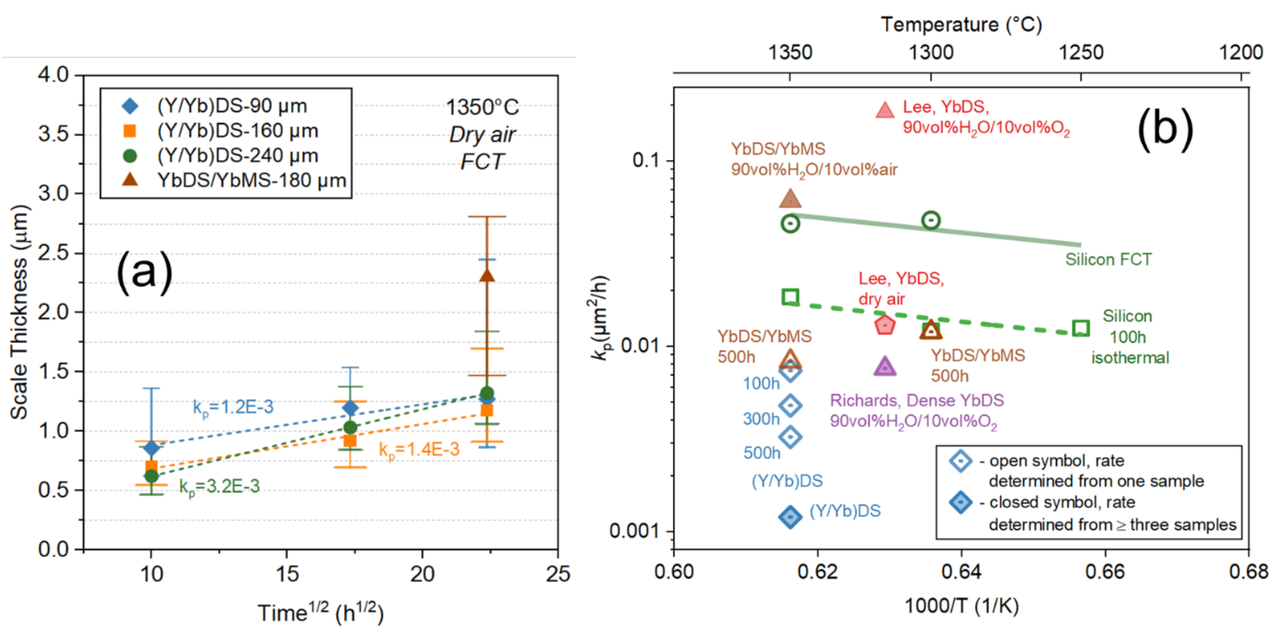

Figure 4 (a) Scale thickness of the (Y/Yb)DS and YbDS/YbMS samples over the course of 1-h FCT in dry air at 1350°C plotted against the square root of time. (b) Arrhenius plot comparing the isothermal and cyclic rates of Si oxidation, the cyclic rates of (Y/Yb)DS-90µm and YbDS/YbMS-180µm, and literature reports of EBC oxidation rates from Richards et al.[24], Lee[23], and Kane et al[20]. All exposures, unless otherwise noted, were performed in dry air.

References

1. Kane KA, Pint BA, Mitchell D, Haynes JA. Oxidation of ultrahigh temperature ceramics: kinetics, mechanisms, and applications. *J Eur Ceram Soc*. 2021.

2. Yin XW, Cheng LF, Zhang LT, Travitzky N, Greil P. Fibre-reinforced multifunctional SiC matrix composite materials. *Int Mater Rev*. 2017;62(3):117–172. https://doi.org/10.1080/09506608.2016.1213939

3. Katoh Y, Snead L. Silicon carbide and its composites for nuclear applications–Historical overview. *J Nucl Mater*. 2019;151849.

4. Opila EJ, Hann RE. Paralinear oxidation of CVD SiC in water vapor. *J Am Ceram Soc*. 1997;80(1):197–205. https://doi.org/10.1111/j.1151-2916.1997.tb02810.x

5. Opila EJ. Oxidation Kinetics of Chemically Vapor-Deposited Silicon Carbide in Wet Oxygen. *J Am Ceram Soc*. 1994;77(3):730–736. https://doi.org/10.1111/j.1151-2916.1994.tb05357.x

6. Opila EJ. Variation of the Oxidation Rate of Silicon Carbide with Water-vapor pressure. *J Am Ceram Soc*. 1999;82(3):625–636.

7. Opila EJ. Oxidation and volatilization of silica formers in water vapor. *J Am Ceram Soc*. 2003;86(8):1238–1248. https://doi.org/10.1111/j.1151-2916.2003.tb03459.x

8. Terrani KA, Pint BA, Parish CM, Silva CM, Snead LL, Katoh Y. Silicon carbide oxidation in steam up to 2 MPa. *J Am Ceram Soc*. 2014;97(8):2331–2352. https://doi.org/10.1111/jace.13094

9. Lee KN, Miller RA. Oxidation Behavior of Mullite-Coated SiC and SiC/SiC Composites under Thermal Cycling between Room Temperature and 1200°-1400° C. *J Am Ceram Soc*. 1996;79(3):620–626.

10. Lee KN, Waters DL, Puleo BJ, *et al.* Development of oxide-based High temperature environmental barrier coatings for ceramic matrix composites via the slurry process. *J Eur Ceram Soc*. 2021;41(2):1639–1653. https://doi.org/10.1016/j.jeurceramsoc.2020.10.012

11. Tejero-Martin D, Bennett C, Hussain T. A review on environmental barrier coatings: History, current state of the art and future developments. *J Eur Ceram Soc*. 2021;41(3):1747–1768. https://doi.org/10.1016/j.jeurceramsoc.2020.10.057

12. Ramasamy S, Tewari SN, Lee KN, Bhatt RT, Fox DS. Mullite-gadolinium silicate environmental barrier coatings for melt infiltrated SiC/SiC composites. *Surf Coatings Technol*. 2011;205(12):3578–3581. https://doi.org/10.1016/j.surfcoat.2010.12.031

13. Lee KN, Fox DS, Eldridge JI, *et al.* Upper temperature limit of environmental barrier coatings based on mullite and BSAS. *J Am Ceram Soc*. 2003;86(8):1299–1306. https://doi.org/10.1111/j.1151-2916.2003.tb03466.x

14. Ramasamy S, Tewari SN, Lee KN, Bhatt RT, Fox DS. Slurry based multilayer environmental barrier coatings for silicon carbide and silicon nitride ceramics - I. Processing. *Surf Coatings Technol*. 2010;205(2):258–265. https://doi.org/10.1016/j.surfcoat.2010.06.029

15. Lee KN, Fox DS, Bansal NP. Rare earth silicate environmental barrier coatings for SiC/SiC composites and Si3N4 ceramics. *J Eur Ceram Soc*. 2005;25(10 SPEC. ISS.):1705–1715. https://doi.org/10.1016/j.jeurceramsoc.2004.12.013

16. Lee KN, Miller RA, Jacobson NS. New generation of plasma-sprayed mullite coatings on silicon carbide. *J Am Ceram Soc*. 1995;78(3):705–710.

17. Lee KN, Zhu D, Lima RS. Perspectives on Environmental Barrier Coatings (EBCs) Manufactured via Air Plasma Spray (APS) on Ceramic Matrix Composites (CMCs): A Tutorial Paper. *J Therm Spray Technol*. 2021;30(1–2):40–58. https://doi.org/10.1007/s11666-021-01168-0

18. Lee KN. Environmental barrier coatings for SiCf/SiC. *Ceram Matrix Compos Mater Model Technol*. 2014;430–451.

19. Padture NP. Environmental degradation of high-temperature protective coatings for ceramic-matrix composites in gas-turbine engines. *npj Mater Degrad*. 2019;3(1). https://doi.org/10.1038/s41529-019-0075-4

20. Kane KA, Pint BA, Stack PIM, Lance MJ, Garcia E. Evaluating steam oxidation kinetics of environmental barrier coatings (JACERS-47841).). *J Am Ceram Soc*. 2021.

21. Harder BJ. Oxidation performance of Si-HfO2 environmental barrier coating bond coats deposited via plasma spray-physical vapor deposition. *Surf Coatings Technol*. 2020;384:125311. https://doi.org/10.1016/j.surfcoat.2019.125311

22. Steibel J. Ceramic matrix composites taking flight at GE Aviation. *Am Ceram Soc Bull*. 2019;98(3):30–33.

23. Lee KN. Yb2Si2O7 Environmental barrier coatings with reduced bond coat oxidation rates via chemical modifications for long life. *J Am Ceram Soc*. 2019;102(3):1507–1521. https://doi.org/10.1111/jace.15978

24. Richards BT, Young KA, De Francqueville F, Sehr S, Begley MR, Wadley HNG. Response of ytterbium disilicate-silicon environmental barrier coatings to thermal cycling in water vapor. *Acta Mater*. 2016;106:1–14. https://doi.org/10.1016/j.actamat.2015.12.053

25. Kane KA, Garcia E, Uwanyuze S, *et al.* Steam oxidation of ytterbium disilicate environmental barrier coatings with and without a silicon bond coat. *J Am Ceram Soc*. 2020;1–16. https://doi.org/10.1111/jace.17650

26. Vaßen R, Bakan E, Sebold D, Sohn YJ. Correlation of process conditions, porosity levels and crystallinity in atmospherically plasma sprayed Yb2Si2O7 environmental barrier coatings. *J Compos Sci*. 2021;5(8). https://doi.org/10.3390/jcs5080198

27. Coatings LPEB, Chen D, Pegler A, Dwivedi G, De Wet D, Dorfman M. Thermal Cycling Behavior of Air Plasma-Sprayed and Low-Pressure Plasma-Sprayed Environmental Barrier Coatings. *Coatings*. 2021;11(7):868.

28. Jian Y, Wang Y, Liu R, Wan F, Zhang J. Property evolutions of Si/mixed Yb2Si2O7 and Yb2SiO5 environmental barrier coatings completely wrapping up SiCf/SiC composites under 1300 °C water vapor corrosion. *Ceram Int*. 2021;47(16):22373–22381. https://doi.org/10.1016/j.ceramint.2021.04.246

29. Bakan E, Marcano D, Zhou D, Sohn YJ, Mauer G, Vaßen R. Yb 2 Si 2 O 7 Environmental Barrier Coatings Deposited by Various Thermal Spray Techniques: A Preliminary Comparative Study. *J Therm Spray Technol*. 2017;26(6):1011–1024. https://doi.org/10.1007/s11666-017-0574-1

30. Olson DH, Deijkers JA, Quiambao-Tomko K, *et al.* Evolution of microstructure and thermal conductivity of multifunctional environmental barrier coating systems. *Mater Today Phys*. 2021;17:100304. https://doi.org/10.1016/j.mtphys.2020.100304

31. Costa GCC, Jacobson NS. Mass spectrometric measurements of the silica activity in the Yb2O3-SiO2 system and implications to assess the degradation of silicate-based coatings in combustion environments. *J Eur Ceram Soc*. 2015;35(15):4259–4267. https://doi.org/10.1016/j.jeurceramsoc.2015.07.019

32. Ridley M, Opila E. Thermochemical stability and microstructural evolution of Yb2Si2O7 in high-velocity high-temperature water vapor. *J Eur Ceram Soc*. 2021;41(5):3141–3149. https://doi.org/10.1016/j.jeurceramsoc.2020.05.071

33. Xu Y, Hu X, Xu F, Li K. Rare earth silicate environmental barrier coatings: Present status and prospective. *Ceram Int*. 2017;43(8):5847–5855. https://doi.org/10.1016/j.ceramint.2017.01.153

34. Felsche J. The crystal chemistry of the rare-earth silicates. *Rare earths*. Springer; 1973:99–197.

35. Turcer LR, Padture NP. Towards multifunctional thermal environmental barrier coatings (TEBCs) based on rare-earth pyrosilicate solid-solution ceramics. *Scr Mater*. 2018;154:111–117. https://doi.org/10.1016/j.scriptamat.2018.05.032

36. Dong Y, Ren K, Lu Y, Wang Q, Liu J, Wang Y. High-entropy environmental barrier coating for the ceramic matrix composites. *J Eur Ceram Soc*. 2019;39(7):2574–2579. https://doi.org/10.1016/j.jeurceramsoc.2019.02.022

37. Sun L, Luo Y, Tian Z, *et al.* High temperature corrosion of (Er0.25Tm0.25Yb0.25Lu0.25)2Si2O7 environmental barrier coating material subjected to water vapor and molten calcium–magnesium–aluminosilicate (CMAS). *Corros Sci*. 2020;175(July):108881. https://doi.org/10.1016/j.corsci.2020.108881

38. Sun L, Luo Y, Ren X, *et al.* A multicomponent γ-type (Gd1/6Tb1/6Dy1/6Tm1/6Yb1/6Lu1/6)2Si2O7 disilicate with outstanding thermal stability. *Mater Res Lett*. 2020;8(11):424–430. https://doi.org/10.1080/21663831.2020.1783007

39. Ridley M, Opila E. Variable thermochemical stability of RE 2 Si 2 O 7 (RE = Sc, Nd, Er, Yb, or Lu) in high-temperature high-velocity steam . *J Am Ceram Soc*. 2021;7. https://doi.org/10.1111/jace.18120

40. Turcer LR, Sengupta A, Padture NP. Low thermal conductivity in high-entropy rare-earth pyrosilicate solid-solutions for thermal environmental barrier coatings. *Scr Mater*. 2021;191:40–45. https://doi.org/10.1016/j.scriptamat.2020.09.008

41. Fernández-Carrión AJ, Alba MD, Escudero A, Becerro AI. Solid solubility of Yb2Si2O7 in β-, γ- And δ-Y2Si2O7. *J Solid State Chem*. 2011;184(7):1882–1889. https://doi.org/10.1016/j.jssc.2011.05.034

42. Wada M, Matsudaira T, Kawashima N, Kitaoka S, Takata M. Mass transfer in polycrystalline ytterbium disilicate under oxygen potential gradients at high temperatures. *Acta Mater*. 2017;135:372–381. https://doi.org/10.1016/j.actamat.2017.06.029

43. Matsudaira T, Wada M, Kawashima N, *et al.* Mass transfer in polycrystalline ytterbium monosilicate under oxygen potential gradients at high temperatures. *J Eur Ceram Soc*.

2021;41(5):3150–3160. https://doi.org/10.1016/j.jeurceramsoc.2020.07.045

44. Wada M, Matsudaira T, Kawashima N, *et al.* Effect of Water Vapor on Mass Transfer in Polycrystalline Yb2Si2O7 under Oxygen Potential Gradients at High Temperatures. *Acta Mater*. 2020;201:373–385. https://doi.org/10.1016/j.actamat.2020.10.002

45. Sullivan RM. Reformulation of oxide growth equations for oxidation of silicon bond coat in environmental barrier coating systems. *J Eur Ceram Soc*. 2019;39(16):5403–5409. https://doi.org/10.1016/j.jeurceramsoc.2019.06.057

46. Singh S, Nganbe M, Chen K. Modeling oxygen permeability through topcoat and thermally grown oxide in dense Yb2Si2O7 environmental barrier coatings. *J Am Ceram Soc*. 2021;(June):1–15. https://doi.org/10.1111/jace.17996

47. Zhao G, Xu B, Ren K, Shao G, Wang Y. Oxygen diffusion through environmental barrier coating materials. *Ceram Int*. 2020;46(11):19545–19549. https://doi.org/10.1016/j.ceramint.2020.05.007

48. Sullivan R. On the Oxidation of the Silicon Bond Coat in Environmental Barrier Coatings. *J Eur Ceram Soc*. 2020;2(February):1–6. https://doi.org/10.1016/j.jeurceramsoc.2020.07.019

49. Kane K, Garcia E, Lance M, Parker C, Sampath S, Pint B. Accelerated oxidation during 1350°C cycling of ytterbium silicate environmental barrier coatings. *J Am Ceram Soc*. 2021;(July):1–10. https://doi.org/10.1111/jace.18231

50. Garcia E, Lee H, Sampath S. Phase and microstructure evolution in plasma sprayed Yb 2 Si 2 O 7 coatings. *J Eur Ceram Soc*. 2019;39(4):1477–1486. https://doi.org/10.1016/j.jeurceramsoc.2018.11.018

51. Kane KA, Stack PIM, Mouche PA, Pillai RR, Pint BA. Steam oxidation of chromium corrosion barrier coatings for sic-based accident tolerant fuel cladding. *J Nucl Mater*. 2021;543. https://doi.org/10.1016/j.jnucmat.2020.152561

52. Su YF, Stack PIM, Stephens CJ, *et al.* Quantifying High Temperature Corrosion. *NACE Corros. 2021*. NACE; 2021:C2021-16805.

53. Deal BE, Grove AS. General relationship for the thermal oxidation of silicon. *J Appl Phys*. 1965;36(12):3770–3778. https://doi.org/10.1063/1.1713945

54. Ogbuji LUJT, Opila EJ. A comparison of the oxidation kinetics of SiC and Si3N4. *J Electrochem Soc*. 1995;142(3):925–930. https://doi.org/10.1149/1.2048559

55. Smialek JL. Compiled furnace cyclic lives of EB-PVD thermal barrier coatings. *Surf Coatings Technol*. 2015;276:31–38. https://doi.org/10.1016/j.surfcoat.2015.06.018

56. Opila EJ. Influence of Alumina Reaction Tube Impurities on the Oxidation of Chemically-Vapor-Deposited Silicion Carbide. *J Am Ceram Soc*. 1995;78(4):1107–1110.

57. Opila EJ, Fox DS, Barrett CA. Cyclic oxidation of monolithic SiC and Si3N4 Materials. *Proc. 17th Annu. Conf. Compos. Adv. Ceram. Mater. Ceram. Eng. Sci. Proc.* Wiley Online Library; 1993:367–374.

58. Kane K, Montoya K, Schappel D, *et al.* Oxidation of 3D-printed SiC in air and steam environments. *J Am Ceram Soc*. 2020;1–13. https://doi.org/https://doi.org/10.1111/jace.17632

59. Kowalski B, Harder B. Thermally grown oxide in water vapor on coated and uncoated SiC. *J Am Ceram Soc*. 2020;103(10):5978–5989. https://doi.org/10.1111/jace.17295